IOP PUBLISHING JOURNAL OF PHYSICS D: APPLIED PHYSICS

J. Phys. D: Appl. Phys. **42** (2009) 145401 (5pp) doi:10.1088/0022-3727/42/14/145401

Direct observation of defects in triple-junction solar cell by optical deep-level transient spectroscopy

Xi Zhang[1], Jianmin Hu[2], Yiyong Wu[2] and Fang Lu[1]

[1] Surface Physics Laboratory, Advanced Materials Laboratory, Fudan University, Shanghai, People's Republic of China

[2] School of Materials Science and Engineering, Harbin Institute of Technology, Harbin, People's Republic of China

E-mail: fanglu@fudan.edu.cn (F Lu)

Received 10 April 2009, in final form 20 May 2009
Published 24 June 2009
Online at stacks.iop.org/JPhysD/42/145401

Abstract

The optical deep-level transient spectroscopy (ODLTS) technique has been used to measure defects in GaInP/GaAs/Ge multi-junction solar cells for the first time. Three modes of ODLTS were used to detect defects in the top two sub-cells of this triple-junction cell separately. For one non-irradiated sample, only one level in the top sub-cell at low temperature was observed. Three samples were irradiated by 100 keV, 130 keV and 170 keV low-energy protons, respectively, and several levels were observed. By computational simulation, the distributions of radiation-induced defects in the samples were given. In the n^+/p GaInP top sub-cells, the levels HT1 and ET1 appeared in both 130 keV and 170 keV proton-irradiated samples. In the n^+/p GaAs middle sub-cells, the level HM1 also appeared in both the samples.

(Some figures in this article are in colour only in the electronic version)

1. Introduction

Multi-junction solar cells are ideal for space applications due to the highest efficiency achieved to date [1]. While the solar cells are applied in space, the study of their degradation induced by irradiation is of practical value, and the deep-level defects induced by irradiation in single-junction solar cells can be easily detected by deep-level transient spectroscopy (DLTS) [2, 3]. However, it is difficult to distinguish the defects in multi-junction solar cells by using the general DLTS [4], because the signals from different sub-cells would mix up, and one could not tell which sub-cell a certain peak in the spectrum belongs to. To date, studies on radiation-induced degradation in multi-junction solar cells have been limited to characterizations such as quantum efficiency [5, 6], electroluminescence [7, 8], current–voltage [6, 9], etc, which are all indirect reflections of radiation-induced defects. Although one could get information on defects in multi-junction cells by measuring single-junction cells to simulate the sub-cells, this is still an indirect way. In this paper, different wavelength semiconductor laser diodes (LDs) are used as an excitation source in DLTS measurement, since the primary character of multi-junction cells is the multi-waveband absorption, which is selective for each sub-cell. Thus, we could choose light with a certain wavelength to directly investigate defects in a certain sub-cell. The defects in non-irradiated and proton-irradiated GaInP/GaAs/Ge triple-junction solar cells have been successfully detected by the ODLTS.

ODLTS is one of the variants of DLTS, and it was first introduced by Mitonneau *et al* [10] to overcome the poor performance of DLTS in measuring minority-carrier defects. The difference between DLTS and ODLTS is in the injection pulse sequence: for ODLTS, carriers are injected into defect levels by optical excitation, which could be either intrinsic [11] or extrinsic [10] excitation, and both majority- and minority-carrier defects could be well observed. In the case of multi-junction solar cells, the experimental arrangement for measuring one sub-cell is the same as that in general ODLTS for single-junction cells, but there are some differences in calculation, and the relative equations will be deduced to explicate our method.

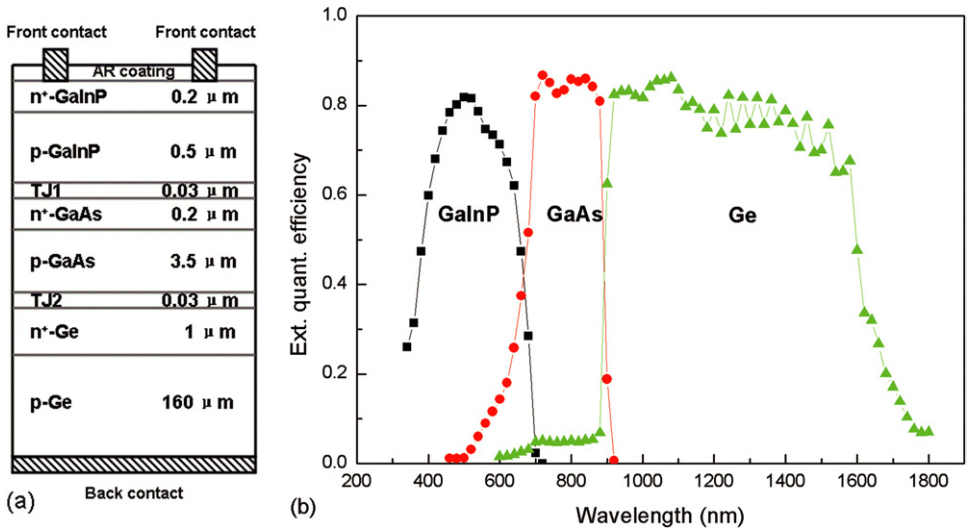

Figure 1. (*a*) Schematic structure of GaInP/GaAs/Ge triple-junction solar cell; (*b*) quantum efficiency of the non-irradiated sample.

2. Principle

In the following deduction, the reference cell structure is set as that of the GaInP/GaAs/Ge triple-junction solar cell in our experiment, which is a typical multi-junction cell and has been described in our previous work [6]. The schematic structure is shown in figure 1(*a*). This cell consists mainly of three sub-cells: n^+/p $Ga_{0.5}In_{0.5}P$ sub-cell (top cell), the electron concentration of the n^+ layer is $2 \times 10^{18}\,cm^{-3}$, the hole concentration of the p layer is $2 \times 10^{17}\,cm^{-3}$; n^+/p GaAs sub-cell (middle cell), the electron concentration of the n^+ layer is $1 \times 10^{18}\,cm^{-3}$, the hole concentration of the p layer is $2 \times 10^{17}\,cm^{-3}$; n^+/p Ge sub-cell (bottom cell). Thus the energy band gap of each sub-cell material decreases step by step from the top to the bottom. The middle cell is connected with the top and bottom cells in series through GaAs tunnel junctions TJ1 and TJ2, respectively. The external quantum efficiency of this triple-junction cell is also given in figure 1(*b*), which shows the absorption edge of each sub-cell and could be taken as a reference for selecting exciting lights in ODLTS measurements.

For triple-junction solar cells, the measured capacitance C could be considered as the total of three barrier capacitances of each sub-cell in series:

$$\frac{1}{C} = \frac{1}{C_t} + \frac{1}{C_m} + \frac{1}{C_b}, \tag{1}$$

where C_t, C_m and C_b are the barrier capacitances of the top, middle and bottom sub-cell, respectively. In ODLTS measurements, the signal is expressed by the capacitance variation ΔC. If ΔC of each sub-cell is small enough, equation (1) could be rewritten as

$$\frac{\Delta C}{C^2} = \frac{\Delta C_t}{C_t^2} + \frac{\Delta C_m}{C_m^2} + \frac{\Delta C_b}{C_b^2}, \tag{2}$$

where ΔC_t, ΔC_m and ΔC_b are the capacitance variations of the top, middle and bottom sub-cell, respectively. To detect defects in the different sub-cells, different measurement modes are set, respectively, as shown in figure 2(*a*).

Mode I is used to detect defects in the top sub-cell, pulsed exciting light is selected with photon energy (653 nm LD, $h\nu = 1.90\,eV$) a little higher than the band gap of the top sub-cell material (GaInP, $E_g = 1.85\,eV$) to make sure that most of the photons are absorbed by this sub-cell; meanwhile the absorption coefficient [12] is small enough to make sure the depletion area is amply illuminated. Thus for mode I $\Delta C_m = 0$, $\Delta C_b = 0$. From equation (2) the measured ODLTS signal is

$$\Delta C^I = \frac{C^2}{C_t^2}\Delta C_t. \tag{3}$$

Due to the proportional relation between ΔC^I and ΔC_t, the levels of defects in the top sub-cell could be calculated in the same way as that in the general DLTS [4], and the concentration of defects in the top sub-cell N_{Tt} is expressed as

$$N_{Tt} = 2\frac{\Delta C_t}{C_t}N_{At} = 2\frac{\Delta C^I}{C}N_{At}\frac{C_t}{C}, \tag{4}$$

where N_{At} is the acceptor concentration on the p side of the top sub-cell. Compared with general DLTS, a coefficient C_t/C is added, so both C and C_t must be obtained to calculate the concentration of the defect.

To detect defects in the middle sub-cell, the exciting light must be selected with photon energy lower than the band gap of the top sub-cell (most photons could get into the middle sub-cell) and higher than the band gap of the middle sub-cell (to avoid photons getting into the bottom sub-cell). Here the 785 nm LD has been used as exciting light, and this mode is defined as mode III. But when the light gets through the top sub-cell, it is possible to excite defects in the top sub-cell by extrinsic excitation. So the measured capacitance variation consists of two parts:

$$\Delta C^{III} = \frac{C^2}{C_t^2}\Delta C_t' + \frac{C^2}{C_m^2}\Delta C_m', \tag{5}$$

where $\Delta C_t'$ and $\Delta C_m'$ are the ODLTS signal excited by the 785 nm LD. Since the ODLTS signal may come from both the

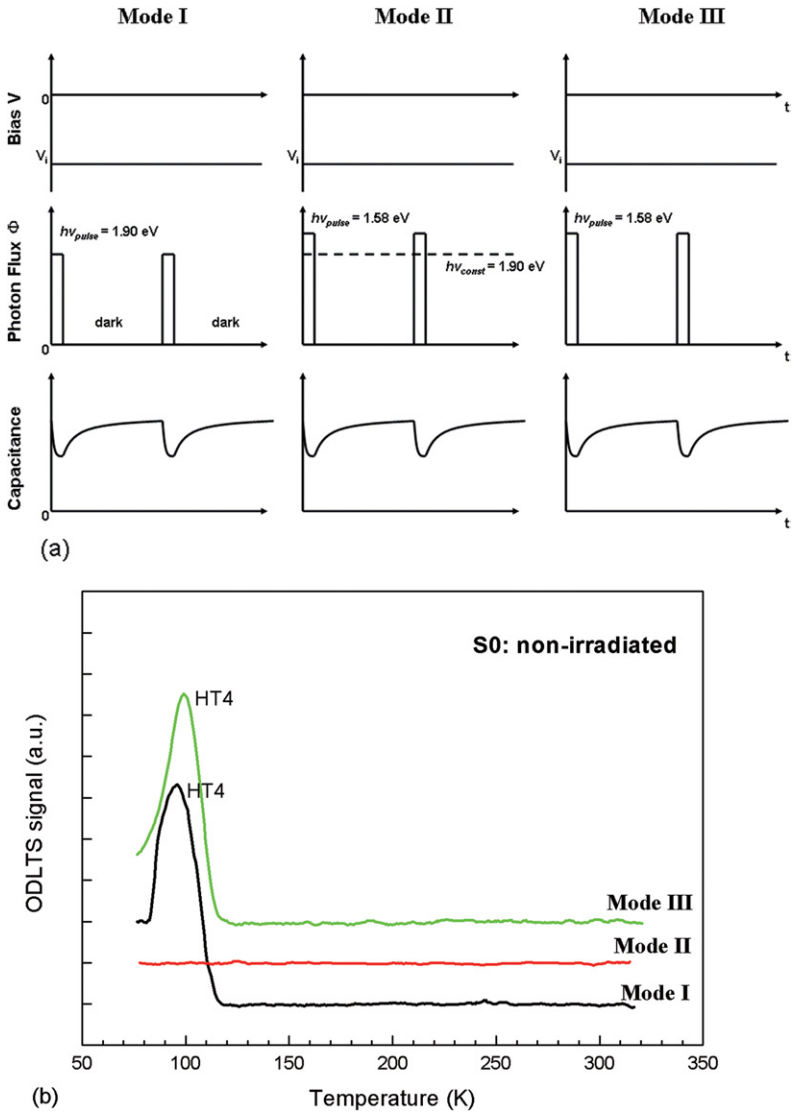

Figure 2. (*a*) Experimental sequences for the three ODLTS modes; (*b*) three modes of ODLTS spectra on the non-irradiated S0 sample. There is an offset between each nearby pair of spectra; all at −0.8 V bias, 4.4 s^{-1} rate window.

top and the middle sub-cells, it is more complicated to analyse the spectra.

In order to remove the effect of extrinsic excitation in the top sub-cell, another 653 nm LD is added as a constant light to make all the defects in the top sub-cell fully filled by the intrinsic excited electrons and holes all the time; meanwhile the 785 nm pulsed exciting light is illuminated to detect defects in the middle sub-cell; this measurement is defined as mode II. In this mode $\Delta C_t = 0$, $\Delta C_b = 0$. Similarly to mode I, the measured capacitance variation and the calculated concentration of the defects are expressed as

$$\Delta C^{II} = \frac{C^2}{C_m^2}\Delta C_m \tag{6}$$

and

$$N_{Tm} = 2\frac{\Delta C_m}{C_m}N_{Am} = 2\frac{\Delta C^{II}}{C}N_{Am}\frac{C_m}{C}, \tag{7}$$

where N_{Am} is the acceptor concentration on the p side of the middle sub-cell. The bottom sub-cell could be detected by a similar method.

3. Experiments

In the ODLTS measurement, capacitance is recorded by a Boonton 7200 capacitance meter, which is controlled by a computer. The sample is put in a cryostat and the temperature changes from 77 to 330 K. Two semiconductor LDs are used as exciting lights with wavelengths 653 nm and 785 nm, respectively. Setups of the three ODLTS modes are shown in figure 2(*a*). Three triple-cell samples were irradiated by protons with different energies at 100 keV (sample S1), 130 keV (sample S2) and 170 keV (sample S3), respectively; the fluence was fixed as 10^{13} cm^{-2}.

4. Results and discussion

The experimental results of a non-irradiated sample (S0) are shown in figure 2(*b*), where the three spectra were measured separately under the three ODLTS modes at the same rate window. It can be seen that no signal could be clearly observed

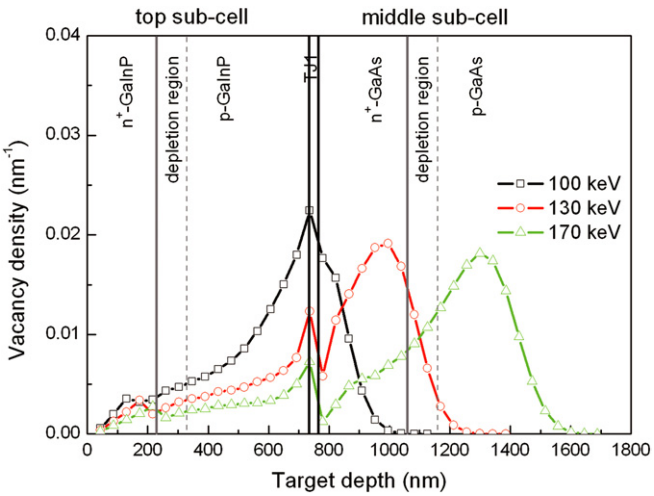

Figure 3. SRIM simulated distribution of vacancy induced by proton irradiation in the GaInP/GaAs/Ge triple-junction solar cell.

under mode II, which means no defect was detected in the middle sub-cell. The spectra under modes I and III are almost the same: there is only one majority peak HT4 (calculated levels: $E_v + 0.07 \pm 0.01$ eV for mode I, $E_v + 0.093 \pm 0.003$ eV for mode III) near 100 K, and the heights of the two peaks are approximately equal. Therefore, the relation between modes I and III could be expressed as

$$\Delta C^{\mathrm{III}} = \frac{C^2}{C_t^2}\Delta C_t' \approx \frac{C^2}{C_t^2}\Delta C_t = \Delta C^{\mathrm{I}}. \qquad (8)$$

This indicates that the same ODLTS results for GaInP are obtained by the two kinds of excitations (intrinsic and extrinsic). However, they are not always the same for all kinds of defects, which may act quite differently for the two exciting lights. In the general case, if $\Delta C_t'$ or $\Delta C_m'$ is not zero under mode III measurement, it would be difficult to calculate the levels of defects.

For the irradiated samples, the distributions of radiation-induced vacancies under different energies in the samples were simulated by the SRIM software [13], as shown in figure 3. The simulation clearly shows that protons with such low energies could not inject into the Ge bottom sub-cell. The depletion regions of sub-cells are marked in figure 3, where the edges at the p sides are marked by two dashed lines, and the defects detected by ODLTS are just near the edges. It can be seen that the concentration of the defects at the depletion region edge (intersection of the two dashed lines and the simulated curve) decreases in the GaInP top sub-cell, but increases in the GaAs middle sub-cell, as the proton energy increases from 100 to 170 keV.

For mode I, the ODLTS spectra of the three irradiated samples at the same rate window are shown in figure 4(*a*), under the same experimental settings as that for sample S0. Three majority and one minority peaks, labelled HT1, HT2, HT3 and ET1, were observed. The corresponding Arrhenius plots and their fitting lines are shown in figure 5, and the calculated results of these energy levels are listed in table 1, where HT1 and ET1 appear in both samples S2 and S3, since

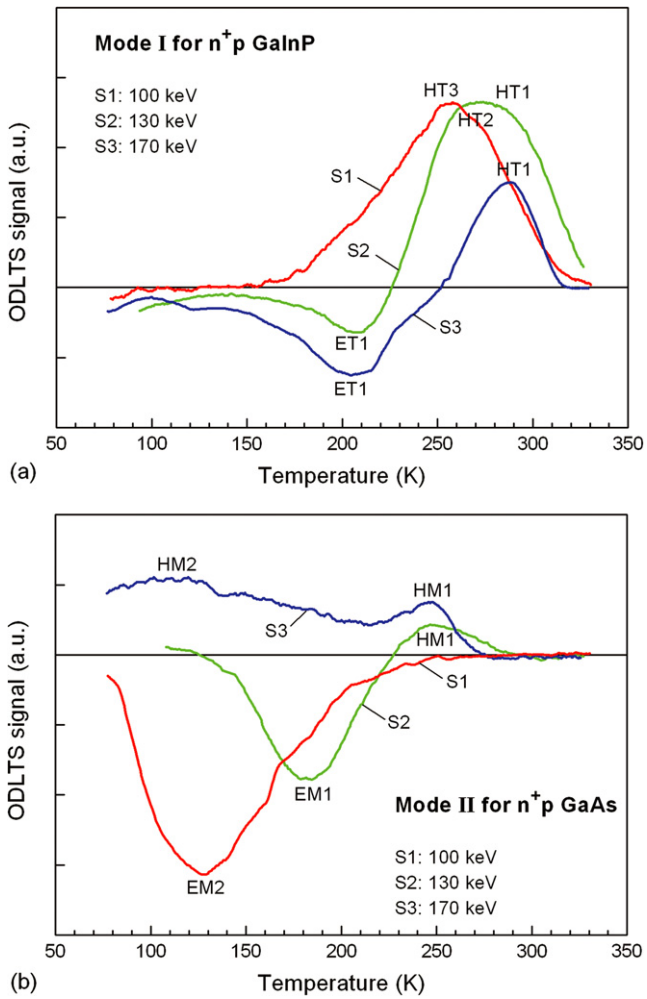

Figure 4. Mode I (*a*) and mode II (*b*) of ODLTS spectra obtained on the three proton-irradiated samples; all at −0.8 V bias, 4.4 s^{-1} rate window.

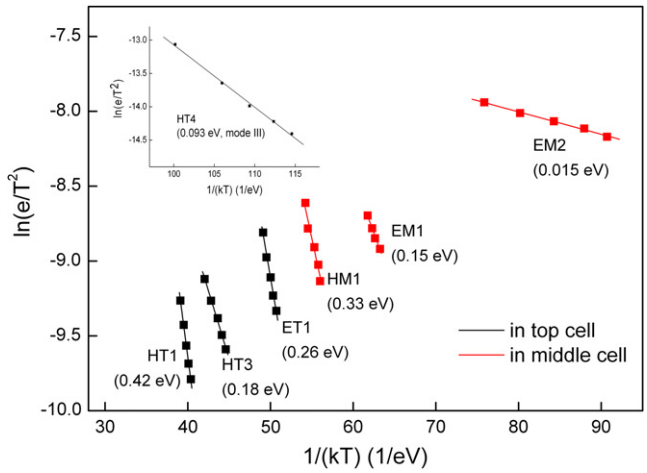

Figure 5. Arrhenius plots and their fitting lines for all the calculated defects levels. The inset is for the defect HT4 in the non-irradiated sample S0.

the calculated values agree well with each other. The wide peak at high temperatures for sample S2 consists of HT1 and HT2, but the proportion of HT2 (by multi-peak fitting) is small and could not be well calculated. Similarly for sample S1, the wide

Table 1. Calculated activation energies (E_a) and concentrations of defects levels in the three proton-irradiated samples under modes I and II. Here the cross section activation energy is not taken into account. The defects levels marked by '—' appeared in the spectra, but the calculation errors for E_a are too large.

	S1		S2		S3	
	E_a (eV)	N_T (cm^{-3})	E_a (eV)	N_T (cm^{-3})	E_a (eV)	N_T (cm^{-3})
HT1			$E_v + 0.42 \pm 0.01$	2.3×10^{16}	$E_v + 0.42 \pm 0.01$	1.8×10^{16}
HT2	—	—	—	—		
HT3	$E_v + 0.18 \pm 0.01$	3.1×10^{16}				
ET1			$E_c - 0.26 \pm 0.02$	8.7×10^{15}	$E_c - 0.26 \pm 0.03$	1.5×10^{16}
HM1			$E_v + 0.33 \pm 0.02$	1.1×10^{16}	$E_v + 0.30 \pm 0.04$	1.8×10^{16}
HM2					—	—
EM1			$E_c - 0.15 \pm 0.01$	4.4×10^{16}		
EM2	$E_c - 0.015 \pm 0.001$	2.3×10^{16}				

peak may also contain HT2. Similarly, in mode II (figure 4(*b*)), HM1, HM2, EM1 and EM2 were observed in the GaAs middle sub-cells. The calculated levels are listed in the lower part of table 1, where EM1 appears in both samples S2 and S3.

With regard to concentration, as the irradiated proton energy increases, there is a tendency for reduction in peak heights for the majority-carrier defects in the top sub-cell, including the disappearance of HT3 (from samples S1 to S2) and HT2 (from samples S2 to S3) and the reduction of HT1 (from samples S2 to S3). In the middle sub-cell, there is a tendency to increase the concentration of the majority-carrier defect HM1 as the proton energy increases. All these seem in agreement with the simulated distribution by SRIM. However, as to the minority-carrier defects, the dependence of concentration on the proton energy does not fit the simulation. This phenomenon indicates that these defects, which we detected, are not simple discrete levels. On the one hand, the defects induced by proton irradiation form some broad bands, and there may be overlapping between majority- and minority-carrier levels, which make the measured concentration lower than the real one induced by proton irradiation. On the other hand, as the proton energy changes, not only the distribution of induced defects changes but also the type of induced defect may change, although the proton energy ranges only from 100 to 170 keV. Just as in mode II, no identical minority-carrier defect was observed in different samples. Thus, the measured concentrations of the defects could not reflect the real radiation-induced defects.

With regard to simulation, in fact, not all the mechanisms could be considered, so only the semi-quantitative analysis is valuable to explicate the phenomenon. And in this paper, the point is that these defects could be detected by the ODLTS method.

5. Conclusion

In summary, defects in GaInP sub-cell and GaAs sub-cell of GaInP/GaAs/Ge triple-junction solar cells (both non-irradiated and proton-irradiated) were measured by the three modes of ODLTS, and their levels and concentrations were calculated. Some defects, HT1, ET1 and EM1, appeared in different samples irradiated by different proton energies, and the calculated levels agree well with each other. By comparing the distribution of radiation-induced defects by SRIM simulation, the component of these observed defects is rather complicated, including overlapping between majority and minority peaks or type-changed defects by varying proton energy or both.

Acknowledgments

This work was supported by special funds from the Major State Basic Research Project, the Commission of Science and Technology of Shanghai and the National Natural Science Foundation of China.

References

[1] Martin A G, Keith E, Yoshihiro H and Wilhelm W 2009 *Prog. Photovolt: Res. Appl.* **17** 85
[2] Dharmarasu N, Yamaguchi M, Bourgoin J C, Takamoto T, Ohshima T, Itoh H, Imaizumi M and Matsuda S 2002 *Appl. Phys. Lett.* **81** 64
[3] Gonzalez M, Andre C L, Walters R J, Messenger S R, Warner J H, Lorentzen J R, Pitera A J, Fitzgerald E A and Ringel S A 2006 *J. Appl. Phys.* **100** 034503
[4] Lang D V 1974 *J. Appl. Phys.* **45** 3014
[5] Sumita T, Imaizumi M, Matsuda S, Ohshima T, Ohi A and Itoh H 2003 *Nucl. Instrum. Methods Phys. Res.* B **206** 448
[6] Hu J M, Wu Y Y, Xiao J D, Yang D Z and Zhang Z W 2008 *Sol. Energy Mater. Sol. Cells* **92** 1652
[7] Zazoui M and Bourgoin J C 2002 *Appl. Phys. Lett.* **88** 4455
[8] Kirchartz T, Rau U, Hermle M, Bett A W, Helbig A and Werner J H 2008 *Appl. Phys. Lett.* **92** 123502
[9] Sharps P R, Aiken D J, Stan M A, Thang C H and Fatemi N 2002 *Prog. Photovolt: Res. Appl.* **10** 383
[10] Mitonneau A, Martin G M and Mircea A 1976 *Proc. 6th Int. Symp. On GaAs and Related Compounds (Edinburgh, UK)* (*Institute of Physics Conference Series No 33a*) p 73
[11] Blondeel A and Clauws P 2000 *Mater. Sci. Eng.* B **71** 233
[12] Adachi S 1989 *J. Appl. Phys.* **66** 6030
[13] Ziegler J F, Ziegler M D and Biersack J P The Stopping and Range of Ions in Matter, SRIM Version: SRIM-2006. 01, downloaded from http://www.srim.org